REPORT DOCUMENTATION PAGE

Form Approved
OMB No. 0704-0188

1. REPORT DATE *(DD-MM-YYYY)*	2. REPORT TYPE	3. DATES COVERED *(From - To)*
10-02-2005	Final	12/20/2001-08/30/2004

4. TITLE AND SUBTITLE

Quantification of the Spatial Variability of the Ocean Surface Roughness and Momentum Flux

5a. CONTRACT NUMBER

5b. GRANT NUMBER

N00173-02-1-G905

5c. PROGRAM ELEMENT NUMBER

6. AUTHOR(S)

Qin Jim Chen

5d. PROJECT NUMBER

5e. TASK NUMBER

5f. WORK UNIT NUMBER

7. PERFORMING ORGANIZATION NAME(S) AND ADDRESS(ES)

Department of Civil Engineering
University of South Alabama
Mobile, AL 36688-0002

8. PERFORMING ORGANIZATION REPORT NUMBER

9. SPONSORING/MONITORING AGENCY NAME(S) AND ADDRESS(ES)

Naval Research Laboratory -SSC
CODE 3235
Stennis Space Center, MS 39529-5004

10. SPONSOR/MONITOR'S ACRONYM(S)

NRL-SSC

11. SPONSOR/MONITOR'S REPORT NUMBER(S)

12. DISTRIBUTION/AVAILABILITY STATEMENT

Approved for Public Release, distribution is unlimited.

13. SUPPLEMENTARY NOTES

14. ABSTRACT

The ocean surface roughness has often been characterized in the literature as being homogeneous in space and time from a large-scale point of view. However, it has been found that the ocean surface roughness is heterogeneous within a wavelength. The surface areas on wave crests are usually rougher than those on wave troughs. The mechanisms range from capillary ripples on wave crests to larger scale wave breaking. Ambient swell and non-uniform currents can also cause significant spatial variations of the surface roughness as short waves become steeper on the swell crest than those on the swell trough. The study parameterizes the spatial variability of the sea surface roughness and quantifies the resultant variations of momentum and energy exchanges between the atmosphere and the coastal ocean using a phase-resolving numerical wave model. Numerical experiments are carried out to test a hypothesis for the suppression of the wave growth rate by the following swell. A simple mechanism is suggested to explain the influence of swell on the short waves observed in the numerical and laboratory experiments.

15. SUBJECT TERMS

Air-sea interactions, wind waves, numerical models, drag coefficient, wind pressure, hydrodynamics

16. SECURITY CLASSIFICATION OF:			17. LIMITATION OF ABSTRACT	18. NUMBER OF PAGES	19a. NAME OF RESPONSIBLE PERSON
a. REPORT	b. ABSTRACT	c. THIS PAGE			Robert W. Galbraith
U	U	U	SAR	23	19b. TELEPHONE NUMBER *(Include area code)* 251-460-6456

Final Report

Quantification of the Spatial Variability of the Ocean Surface Roughness and Momentum Flux

Qin Jim Chen
Department of Civil Engineering
University of South Alabama
Mobile, AL 36688-0002

October 2004

ABSTRACT

It is well known that physical processes occurring at the air-sea interface, such as air-sea mass, momentum and energy exchanges, are controlled by the ocean surface roughness that has often been characterized in the literature as being homogeneous in space and time from a large-scale point of view. However, the ocean surface roughness is heterogeneous within a wavelength. The surface areas on wave crests are usually rougher than those on wave troughs. The mechanisms range from capillary ripples on wave crests to larger scale wave breaking. Ambient swell and non-uniform currents can also cause significant spatial variations of the surface roughness as short waves become steeper on the swell crest than those on the swell trough. The study parameterizes the spatial variability of the sea surface roughness and quantifies the resultant variations of momentum and energy exchanges between the atmosphere and the coastal ocean using a phase-resolving numerical wave model. Numerical experiments have been carried out to test a hypothesis for the suppression of the wave growth rate by the following swell. A simple mechanism is suggested to explain the influence of swell on the short waves observed in the numerical and laboratory experiments.

TABLE OF CONTENTS

1.0 INTRODUCTION

Many naval operations occur over and in the atmosphere-ocean interface. The success of such operations depends on the understanding of the structure and behavior of the air-sea interface. It is well known that many physical processes occurring at the air-sea interface, such as air-sea mass, momentum and energy exchanges, are controlled by the ocean surface roughness that has often been characterized in the literature as being homogeneous in space and time from a large-scale point of view. Recently, it is realized, however, that the utilization of remote sensing techniques for the study of the air-sea interface requires the in-depth understanding of the spatial and temporal variability of the ocean surface roughness at multiple scales.

The ocean surface roughness is indeed inhomogeneous within a wavelength. The surface areas on wave crests are usually rougher than those on wave troughs. The mechanisms range from capillary ripples on wave crests to larger scale wave breaking (see e.g., Longuet-Higgins, 1963; Jiang et al., 1999; Ducan et al., 1999). An ambient swell or current can also cause significant spatial variations of the surface roughness as short waves become steeper on the swell crest than those on the swell trough (Longuet-Higgins and Stewart, 1960). The purpose of the proposed study is to quantify the spatial variability of the ocean surface roughness and the resultant variations of momentum and energy exchanges between the atmosphere and the ocean using a phase-resolving numerical wave model.

The report is organized as follows. First, we present the new parameterization of the momentum flux transferred from the wind to surface gravity waves in the coastal zone. Next, we analyze the effect of wave nonlinearity on the drag coefficient using Stokes' second-order wave theory. After that, we show how to implement the parameterized wind stress into the phase resolving Boussinesq wave model with enhanced dispersion properties. Then tests of the extended Boussinesq model with the wind forcing against wave measurements in a shallow lake are carried out followed by an application of the model to the study of sea-swell interactions. Finally, we summarize the findings of the project.

2.0 HETEROGENEOUS AIR-SEA MOMENTUM FLUX

2.1 Parameterization of Momentum Flux

The momentum flux transferred from winds to surface waves in the time-domain Boussinesq wave model may be parameterized as the wind stress, $\boldsymbol{\tau} = \rho_a C_d \boldsymbol{U}|\boldsymbol{U}|$, where $\boldsymbol{U}$ is the wind velocity vector at a reference elevation, and C_d is the corresponding drag coefficient. Suggested by the field evidence, the wind drag coefficient in the coastal zone must be a function of not only the wind speed, but also the geometry of the surface gravity waves that are often skewed and asymmetrical owing to the seabed boundary. We propose a new formula of drag coefficient as follows.

$$C_d 10^3 = (a_1 + a_2 |\eta_x|) + bU_{10} \qquad (1)$$

where a_1, a_2 and b are empirical coefficients, and η_x is the instantaneous surface slope computed in the Boussinesq model. Phase average of the drag coefficient allows for a comparison of the new

formula with conventional drag coefficient formulas, such as the equation proposed by Wu (1980).

Figure 1 illustrates the phase-averaged drag coefficient as a function of wind speed and wave steepness, ka (k = wave number and a = wave amplitude). We choose a_1=0.2, a_2=18, and b=0.065. The wave steepness ranges from 0.05 to 0.2 with an increment of 0.05. It is seen that the new drag coefficient increases with both wind speed and wave steepness. Following Wu (1980), the third term in Equation (1) is set to be 0.4875 for wind speed less than 7.5m/s. The dashed line in Figure 1 depicts the drag coefficient given by Wu

$$C_d 10^3 = 0.8 + 0.065 U_{10} \tag{2}$$

which is only a function of wind speed. The curves of the new drag coefficient are parallel to Wu's curve and the offset depends on the wave steepness.

In addition to Wu (1980)'s equation, a large number of empirical formulas for the drag coefficient have been proposed in the literature (see e.g. Geernaert, 1990). Each formula represents the best fit to a specific dataset. Figure 2 shows a comparison of the new drag coefficient and the existing formulations. It is seen that the scattering of the drag coefficient as a function of the wind speed may be explained by the effect of the sea state, or the wave steepness. Statistically, Equation (1) agrees fairly well with all the data, which is not achieved by any single existing formula of drag coefficient.

One of the crucial differences in airflow over steep surface waves in comparison to the flow over a flat surface is the presence of a form drag due to the separation of airflow. Laboratory measurements of the tangential and normal stresses on the air-water interface (Banner and Peirson, 1998) suggest that the form drag accounts for the major proportion of the wind stress once the waves have developed beyond their early growth stage. The most interesting scenario of wind effects on coastal waves is the strong wind condition. We hypothesize that the separation of airflow occurs on the lee side of the wave crest in the shallow water and, consequently, the form drag is a dominant contributor to the momentum flux between the atmosphere and the nearshore wave field. The hypothesis is in line with the sheltering theory proposed by Jeffreys (1925) as a mechanism of wave generation.

The time-domain Boussinesq model resolves the individual wave motion and predicts reasonably well the geometry of the surface waves distorted by the seabed, such as the skewness and asymmetry of the waves in the shallow water (e.g. Chen et al., 2000 and Shi et al. 2003). The wind stress implemented into the Boussinesq model should vary over a wavelength, with a larger drag coefficient on the wave crest than that in the trough to take the form drag into account. In fact, only the heterogeneous distribution of the wind stress over a wavelength allows for changes of wave height by a wind in a phase-resolving wave model. Assuming that the form drag is dominant over the skin friction, we apply the wind stress on the wave crest only, neglecting the effect of the shear stress on the wave trough in the Boussinesq model.

The temporal and spatial variation of drag coefficient is one of the important features of the wind stress on the nearshore waves simulated by the phase-resolving Boussinesq model. With the instantaneous wave celerity and wave slope obtained from the computed surface elevation at each grid and every time step, the wind stress is calculated as a function of the wind velocity relative to the

wave celerity as well as the wave slope in the following form

$$\tau = C_d \rho_a \mid U_{10} - C \mid (U_{10} - C) \tag{3}$$

where C is the instantaneous wave celerity estimated in the Boussinesq model. Equation (3) is similar to the wind stress formulation followed by Schwab et al. (1984) in a wave prediction model on the basis of a phase-averaged momentum balance equation rather than an energy balance equation.

2.2 Effects of Wave Nonlinearity on the Drag Coefficient

The new formulation of wind drag coefficient introduced in the preceding section depends on the wave steepness and becomes effective only on the wave crest. It is well known that the effects of wave nonlinearity increase the wave steepness and result in peaky wave profiles. We shall analyze the effect of wave nonlinearity on the drag coefficient given by Equation (1) using Stokes' second-order wave theory.

The free surface profile given by Stokes' second-order theory reads

$$\eta = a\cos(kx - \omega t) + \frac{a^2 k}{4}\frac{(2+\cosh 2kh)\cosh kh}{\sinh^3 kh}\cos 2(kx - \omega t) \tag{4}$$

where a is the first-order (linear) amplitude of the free-surface disturbance, $k=\frac{2\pi}{L}$ is the wave number, h is the still water depth, L is the wave length, x is the horizontal distance, t is time, and ω is the angular frequency. At t = 0 and in the deep water ($h>>L/2$), Equation (4) may be simplified as

$$\eta = a\cos kx + \frac{a^2 k}{2}\cos 2kx \tag{5}$$

Upon the use of the trigonometric identity and rearrangement of Equation (5), we obtain

$$\eta k = a^2 k^2 \cos^2 kx + ak\cos kx - \frac{a^2 k^2}{2} \tag{6}$$

Because the wind stress (or drag coefficient) is only applied on the wave crest above the still water level, we need to find out the length of the wave crest. Solving Equation (6) with $\eta k = 0$ yields

$$x_0 k = \arccos f(ak) \tag{7}$$

in which

$$f(ak) = -\frac{1}{2ak} + \sqrt{(\frac{1}{2ak})^2 + \frac{1}{2}} \tag{8}$$

Integrating the drag coefficient over a wave length leads to the phase-averaged drag coefficient

$$\overline{C}_d = \frac{1}{L}\int_{L-x_0}^{L+x_0} C_d dx = \frac{a_1}{\pi} kx_0 + \frac{a_2}{\pi} k\eta_{\max} + \frac{b}{\pi} kx_0 U_{10} \qquad (9)$$

where $\eta_{\max}$ is the surface elevation at the wave crest. For linear waves, we have $x_0 = \frac{L}{4}$ and $\eta_{\max} = a$.

The ratio of the drag coefficient on a Stokes' second-order wave profile to that on a linear wave profile is given by

$$\frac{\overline{C}_d}{(\overline{C}_d)_{linear}} = 1 + \frac{(a_1 + bU_{10})(2kx_0 - \pi) + a_2(ka)^2}{(a_1 + bU_{10})\pi + 2a_2 ka} \qquad (10)$$

Figure 3 illustrates the variation of such a ratio as a function of wave steepness and wind speed. It is seen that the wave nonlinearity can increase the phase-averaged drag coefficient by 10-15 percent.

AN ADVANCED BOUSSINESQ WAVE MODEL WITH WIND FORCING

The formulation of the wind stress is implemented into the Boussinesq wave model developed by Wei et al. (1995), Kennedy et al. (2000), Chen et al (2000), and Chen et al. (2003). In order to take into account the short waves generated by local winds, we also extend the dispersion accuracy of the one-dimensional version of the model to $kh = 6$ (h = still water depth) by introducing the additional terms from Madsen and Schaffer's (1998) equations into the model. A new set of coefficients for better shoaling properties of the equations (Madsen, 2002, personal communication, and Kennedy et al, 2002) is also implemented into the model. In one horizontal dimension, the extended Boussinesq equations read

$$\eta_t + M_x = 0 \qquad (11)$$

where

$$M = (h+\eta)\left[u_\alpha + \left(\frac{z_\alpha^2}{2} - \frac{1}{6}\left(h^2 - h\eta + \eta^2\right)\right)u_{\alpha xx} + \left(z_\alpha + \frac{1}{2}(h-\eta)\right)(hu_\alpha)_{xx}\right] + (\beta_2 - \beta_1)h^2\left((h+\eta)u_\alpha\right)_{xx} - \beta_2\left(h^2\left((h+\eta)u_\alpha\right)_x\right)_x + (\beta_2 - \beta_1)h^2\eta_{xt} - \beta_2\left(h^2\eta_t\right)_x \qquad (12)$$

and

$$u_{\alpha t} + u_\alpha u_{\alpha x} + g\eta_x + \Lambda_0 + \Lambda_1 + \Lambda_2 + \Lambda_3 - R_b - R_s + R_f - R_w = 0 \qquad (13)$$

where

$$\Lambda_0 = \left(\frac{z_\alpha^2}{2} + (\alpha_2 - \alpha_1)h^2\right)u_{\alpha xxt} + (z_\alpha - \alpha_2 h)(hu_{\alpha t})_{xx} + (\alpha_2 - \alpha_1)h^2\eta_{xxx} - \alpha_2 h(h\eta_x)_{xx} \qquad (14)$$

$$\Lambda_1 = \left[z_\alpha u_\alpha (hu_\alpha)_{xx} + \frac{1}{2} z_\alpha^2 u_\alpha u_{\alpha xx} - \eta (hu_{\alpha t})_x + \frac{1}{2} ((hu_\alpha)_x)^2 \right]_x + \frac{1}{2}(\alpha_2 - \alpha_1) h^2 (u_\alpha^2)_{xxx} - \frac{1}{2} \alpha_2 h \left(h (u_\alpha^2)_x \right)_{xx} \tag{15}$$

$$\Lambda_2 = \left[\eta u_{\alpha x} (hu_\alpha)_x - \eta u_\alpha (hu_\alpha)_{xx} - \frac{1}{2} \eta^2 u_{\alpha xt} \right]_x \tag{16}$$

$$\Lambda_3 = \left[\frac{1}{2} \eta^2 (u_{\alpha x})^2 - \frac{1}{2} \eta^2 u_\alpha u_{\alpha xx} \right]_x \tag{17}$$

In the equations, η is the free surface elevation relative to the still water level; u_α is the velocity at the reference elevation z_α (= - 0.54122h) in the water column; and the subscripts t and x denote time and spatial differentiations, respectively. The dispersion enhancement coefficients with improved shoaling properties are $(\beta_1, \beta_2) = (0.03917, 0.315236)$ and $(\alpha_1, \alpha_2) = (0.01052, 0.124537)$. The additional terms, R_b, R_s, R_f, and R_w represent the effects of wave breaking, subgrid lateral turbulent mixing, seabed shear stress, and wind stress, respectively. Detailed descriptions of the first three terms can be found in Chen et al. (1999). Upon the use of Equation (3), we obtain

$$R_w = \frac{\rho_a}{\rho(h+\eta)} C_d \, | U_{10} - C | \, (U_{10} - C) \tag{18}$$

where ρ is the water density.

The internal wave-maker for the generation of random waves at the offshore boundary is extended to accommodate the enhancement of dispersion properties in the Boussinesq equations. In comparison to Wei et al.'s (1995) model, the additional terms in Equation (12) requires the solution of a tridiagonal system for the continuity equation.

Other extensions of the model include the modification of the breaking criteria in the model to account for the energy dissipation owing to whitecaps. The original breaking criteria in Kennedy et al. (2000) were designed for depth-limited wave breaking. The basic idea is to replace the still water depth h by C^2/g where g is the gravitational acceleration. This leads to the modified criteria for the onset ($\eta_t^{(I)}$) and cessation ($\eta_t^{(F)}$) of wave breaking as follows

$$\eta_t^{(I)} = \gamma_1 C \qquad \eta_t^{(F)} = \gamma_2 C \tag{19}$$

in which γ_1 =0.35~0.65 and γ_2 =0.15. We choose the lower limit of γ_1 in the presence of a wind that is in the direction of the wave train. Other terms with h in the breaking scheme of Kennedy et al. (2000) are also modified in a similar fashion.

4.0 MODELING WAVE GROWTH ON A SHALLOW LAKE

The test cases in Chen et al. (2002) were focused on the surface roughness length and drag coefficient associated with shoaling waves over a distance of about 500m. Can the wind stress implemented into the Boussinesq model simulate the growth of wind waves over a longer fetch? We shall address such a question using the data set of wave growth in Lake George, Australia collected by Young and Verhagen (1996).

Lake George is a shallow lake with a typical water depth of 2m. It is about 20km long and 10km wide. A series of eight observation stations were deployed along the north-south fetch to measure the wind waves. The wave data collected by Young and Verhagen (1996) under a nearly ideal condition have served as a test bed for a number of phase-averaged wave models, such as SWAN (Simulating WAves Nearshore, Booij et al., 1999). We choose two data sets corresponding to a medium wind speed of U_{10} = 10.8m/s and a large wind speed of U_{10} = 15.2m/s to test the wind stress formulation incorporated into the Boussinesq model. Owing to the dispersion limit of the Boussinesq model ($kh < 6$), only the observations at the last four stations (5-8) are utilized. The fetch between Stations 5 and 8 is about 4.25 km. The up-wave boundary condition is taken from the observation at Station 5 where the zero-moment wave height is H_{mo} = 0.367m and the peak wave period is T_p = 2.34s in the case of a moderate wind (U_{10} = 10.8m/s), and H_{mo} = 0.473m and T_p = 2.4s in the case of a strong wind (U_{10} = 15.2m/s). We use *TMA* shallow water wave spectra (Bouws et al., 1985) with the shape parameter γ = 3.3 at the up-wave boundary as the input to the Boussinesq model. A bottom friction coefficient of f = 0.0005 is used in the quadratic law of the bottom shear stress (Chen et al., 1999).

Figure 4 shows comparisons of the computed and measured significant wave heights as well as the computed and inferred drag coefficients under the moderate wind condition. It is seen that the wave heights predicted by the Boussinesq model are in fairly good agreement with the field measurements. The computed peak wave periods, however, do not agree with the observations. The wind stress incorporated into the Boussinesq model simply does not lead to the increase of wave period along the fetch. The downshift of the peak frequency is absent in the modeled wave energy spectrum. This is attributed to the inability of the one-dimensional Boussinesq model to take quadruplet interactions into account. Interestingly, the phase-averaged drag coefficient calculated from the Boussinesq model is in good agreement with the coefficient estimated using the modeled wave characteristics and Anctil and Donelan's (1996) formula. The drag coefficients given by Taylor and Yelland's (2001) formula (triangles), however, are smaller than either Boussinesq or Anctil and Donelan's result (solid line and squares).

Similar comparisons are made for the case of large wind speed as shown in Figure 5. Again, the Boussinesq model predicts the growth of wave height fairly well in comparison to the field measurements but considerably under-predicts the increase of wave period. The agreement among the drag coefficients is also very similar to the case with a moderate wind. The phase-averaged drag coefficient obtained from the Boussinesq model agrees better with Anctil and Donelan's result than does Taylor and Yelland's formula, as shown in Figure 5b. Notice that all the drag coefficients are computed using the wave field given by the one-dimensional Boussinesq model, which is not able to predict the downshift of the peak frequency. Nevertheless, the prediction of wave height growth under

both moderate and strong wind conditions by the Boussinesq model confirms that the new formulation of wind stress is a good representation of the momentum flux transferred from a wind to surface waves in a phase-resolving model.

5.0 THE INFLUENCE OF SWELL ON THE GROWTH OF WIND WAVES

Donelan (1987) among others has found that the addition of mechanically-generated swell to the wind waves in a wave flume results in a pronounced reduction in the energy of the wind sea while the swell gains significant energy from the following wind in comparison to pure wind waves. Although a number of hypotheses have been proposed in the literature, the attenuation mechanism for the wind sea owing to the presence of swell is still poorly understood. As demonstrated in the preceding section, the extended Boussinesq model is able to simulate the growth of wave energy for a given wind speed and a non-zero wave spectrum at the up-wave boundary. We shall conduct a series of numerical experiments to examine how swell influences the growth rate of wind waves on the basis of the extended Boussinesq wave model with the wind forcing. The Lake George case with a moderate wind is used as a reference for comparisons.

Figure 6 depicts snapshots of the computed free surface elevations of the cases with and without swell. The right panel corresponds to the first case with a moderate wind speed in the preceding section. A monochromatic, long wave train with a period of three times the peak wave period of the short waves is imposed at the up-wave boundary in addition to the wind waves, as shown in the right panel. The wave height of the swell is 0.184 m. Each snapshot (e.g. A to F) in each panel is 15 minutes apart, beginning 15 minutes after the model starts.

Figure 7 shows the energy density spectra of the modeled sea surface with and without swell. The dashed lines represent the spectra at the up-wave boundary while the solid lines are the spectra 4 km down-wind. In contrast to the spectra of the pure wind waves on the right, the left panel shows that the short waves barely grow while the swell gains energy from the wind. The Boussinesq model qualitatively reproduces what Donelan (1987) observed in the laboratory about the suppression of the wave growth rate in the presence swell under field conditions. No field measurements of sea-swell interaction, however, are available for a direct test of the influence of swell predicted by the Boussinesq wave model with the wind forcing.

The slope of the sea surface is a measure of the surface roughness. Figure 8 illustrates spectra of the modeled sea surface slope with and without swell. The dashed lines represent the slope spectra at the up-wave boundary while the solid lines are the spectra 4 km down-wind. A comparison of the left and right panels shows that the swell actually reduces the growth rate of the surface slope, or the sea surface roughness of the short waves. This is consistent with the suppression of the short-wave energy growth rate by the following swell.

Figure 9 depicts the spatial variations of the wave height and phase-averaged drag coefficient with and without swell. The solid lines denote the model result of pure wind waves while the dashed lines are the result of combined sea and swell. It is seen that the presence of swell yields a slightly smaller growth rate of the total wave energy than that of the pure sea. A similar trend is found in the phase-

averaged drag coefficient, as shown on the right. To examine the effect of the swell steepness on the growth rate of the wind waves, we reduce the swell amplitude to 0.041 m, and repeat the simulation above without changing other conditions. The Boussinesq model predicts that the smaller the swell steepness, the less degree the suppression of the shore-wave growth rate, as seen by a direct comparison of Figure 7 and Figure 10.

The numerical results suggest that on the swell crests, the larger surface roughness and the sheltering effect lead to a larger momentum transfer than that on the swell trough, but the momentum/energy flux averaged over the swell wavelength remains relatively unchanged. The majority of the short waves riding on the swell crest are subjected to the swell-induced form drag owing to the sheltering effect and a homogeneous wind stress over an entire short wavelength prevents the short wave from growing. Therefore, the swell takes advantage of the stronger momentum flux on its crest and harvests most of the energy transferred from the wind to the water. In layman's words, the finite amplitude swell serves as a "master" wave and the wind waves riding on the swell act as "slaves" for momentum transfer. Consequently, the swell amplitude increases while the wind sea barely grows.

6.0 SUMMARY AND CONCLUSIONS

A phase-resolving wind stress formula has been developed, analyzed and applied. The report documents (1) the parameterization of the momentum flux transferred from the wind to surface gravity waves in a phase-resolving Boussinesq wave model, (2) the analysis of the effect of wave nonlinearity on the drag coefficient based on Stokes' second-order wave theory, (3) tests of the extended Boussinesq model with the wind forcing against wave measurements in a shallow lake, and (4) numerical experiments on the influence of swell on the growth rate of the wind waves. Fairly good agreement between the modeled wave heights and field data has been found. A new, simple mechanism has been suggested to explain the suppression of the wind wave growth rate in the presence of swell. Results of the study have been published in the Journal of Waterway, Port, coastal and Ocean Engineering (Chen et al. 2004a) and the International Conference on Coastal Engineering (Chen et al. 2002 and Chen et al. 2004b).

The methodology for the parameterization of the phase-resolving air-sea momentum flux as well as the extended Boussinesq wave model incorporating the wind effects appear to be a promising tool for the study of sea-swell-wind interactions and wind effects on nearshore wave propagation. However, the limit of the dispersion accuracy to $kh < 6$ prevents the extended Boussinesq wave model from being compared directly with existing laboratory datasets on the influence of swell on the growth of wind waves. Thus, it is recommended that state-of-the-art Boussinesq models with the dispersion accuracy up $kh = 40$ (e.g. Madsen et al., 2002) be employed for the study of sea-swell-wind interactions in the future.

7.0 ACKNOWLEDGEMENTS

This study was supported by the Naval Research Laboratory through Grant N00173-02-1-G905.

8.0 REFERENCES

Anctil, F., and Donelan, M. A. (1996). "Air-water momentum flux observations over shoaling waves." *J. Phys. Oceanogr.* 26: 1344-1353.

Banner, M. L., and Peirson, W. L. (1998). "Tangential stress beneath wind driven air-water interfaces." *J. Fluid Mech.*, 364, 115-145.

Booij, N., Ris, R. C., and Holthuijsen, L. H. (1999). "A third-generation wave model for coastal regions. Part 1, Model description and validation." *J. Geophys. Res.*, C4, 104, 7649-7666.

Bouws, E., Gunther, H., Rosenthal, W., and Vincent, C. L. (1985). "Similarity of the wind wave spectrum in finite depth water." *J. Geophys. Res.*, 90, 975-986.

Chen, Q., Dalrymple, R. A., Kirby, K. T., Kennedy, A. B., and Haller, M. C. (1999). "Boussinesq modeling of a rip current system." *J. Geophys. Res.*, 104 (C9): 20,617-20,637.

Chen, Q., Kirby, J. T., Dalrymple, R. A., Kennedy, A. B., and Chawla, A. (2000). "Boussinesq modeling of wave transformation, breaking and runup. II: 2D." *Journal of Waterway, Port, Coastal and Ocean Engineering*, 126, 48-56.

Chen, Q., Kaihatu, J. M., Hwang, P. A. and Douglass, S. L., (2002). "Quantification of the wind effect on wave breaking based on a Boussinesq wave model." *Proceedings 28th International Conference on Coastal Engineering*, 332-343.

Chen Q., Kirby, K. T., Dalrymple, R. A., Shi, F., and Thornton, E. B. (2003). "Boussinesq modeling of longshore currents." *J. Geophys. Res.* In press.

Chen, Q., Kaihatu, J. M. and Hwang, P. A., (2004a). "Incorporation of the wind effects into Boussinesq wave models." *Journal of Waterway, Port, Coastal and Ocean Engineering.* 130, 312-321.

Chen Q., Hwang, P. A., Kaihatu, J. M., (2004b). "The influence of swell on the sea surface roughness and the growth of wind waves." *Proceedings 29th International Conference on Coastal Engineering.* In press.

Donelan, M. A., (1987). "The effect of swell on the growth of wind waves." *Johns Hopkins APL Technical Digest*, 8 (1): 18-23.

Duncan, J. H., Qiao, H., Philomin, V. and Wenz, A., (1999). "Gentle spilling breakers: crest profile evolution." *J. Fluid Mech.*, 379: 191-222.

Geernaert, G. L. (1990). "Bulk parameterizations for the wind stress and heat fluxes." *Surface Waves and Fluxes*, Edited by G. L. Geernaert and W. J. Plant. Kluwer Academic Publishers. Vol. 1, 91-172.

Hatori, M., Tokuda, M. and Toba, Y., (1981). "Experimental study on strong interactions between regular waves and wind waves." *J. Oceanogr. Soc. Japan,* 37, 111-119.

Jeffereys, H. (1925). "On the formation of waves by wind. II." *Proc. Roy. Soc. A*, 110, 341-347.

Jiang, L., Lin, H., Schultz, W. W., and Perlin, M., (1999). "Unsteady ripple generation on steep gravity-capillary waves." *J. Fluid Mech.*, 386: 281-304.

Kennedy, A. B., Chen, Q., Kirby, J. T., and Dalrymple, R .A. (2000). "Boussinesq modeling of wave transformation, breaking and runup. I: 1D." *Journal of Waterway, Port, Coastal and Ocean Engineering*, 126: 39-47.

Kennedy, A. B., Kirby, J. T., and Gobbi, M. F. (2002). "Simplified higher-order Boussinesq equations I. Linear simplifications." *Coastal Engineering*, 44, 205-229.

Longuet-Higgins, M. S. and Stewart, R. W., (1960). "Changes in the form of short gravity waves on long waves and tidal currents." *J. Fluid Mech.*, 8: 565-585.

Longuet-Higgins, M. S., (1963). "The generation of capillary waves by steep gravity waves." *J. Fluid Mech.*, 16: 138-159.

Madsen, P. A., and Schaffer, H. A. (1998). "Higher order Boussinesq-type equations: Derivation and analysis." *Philosophical Trans. Royal Soc.*, 356, 3123-3184.

Madsen, P. A., Bingham, H. B., and Liu, H. (2002). "A new Boussinesq model for fully nonlinear waves from shallow to deep water." *J. Fluid Mech.*, 462, 1-30.

Schwab, D. J., Bennett, J. R., Liu, P. C., and Donelan, M. A. (1984). "Application of a simple numerical wave prediction model to Lake Erie." *Journal Geophysical Research.* 89 (C3), 3586-3592.

Shi, F., Kirby, J. T., Dalrymple, R. A., and Chen, Q. (2003). "Wave simulations in Ponce de Leon inlet using a Boussinesq model." *Journal of Waterway, Port, Coastal and Ocean Engineering.* 129, 124-135.

Taylor, P. K., and Yelland, M. J. (2001) "The dependence of sea surface roughness on the height and steepness of the waves." *J. Phys. Oceanogr.* 31: 572-590.

Wei, G., Kirby, J. T., Grilli, S. T., and Subramanya, R. (1995). "A fully nonlinear Boussinesq model for surface waves. Part 1: Highly nonlinear unsteady waves." *J. Fluid Mech.*, 294, 71-92.

Wu, J. (1980). "Wind-stress coefficient over the sea surface near neutral conditions-A revisit." *J. Phys. Oceanogr.* 10: 727-740.

Young, I. R and Verhagen, L. A. (1996). "The growth of fetch limited waves in water of finite depth. Part 1: Total energy and peak frequency." *Coastal Engineering.* 29, 47-78.

9.0 APPENDIX

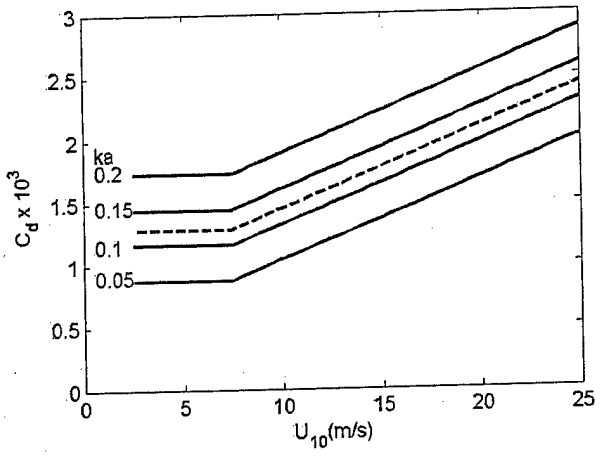

Fig. 1 Drag coefficient as a function of wind speed and wave steepness (solid lines). The dashed line is Wu's (1980) drag coefficient.

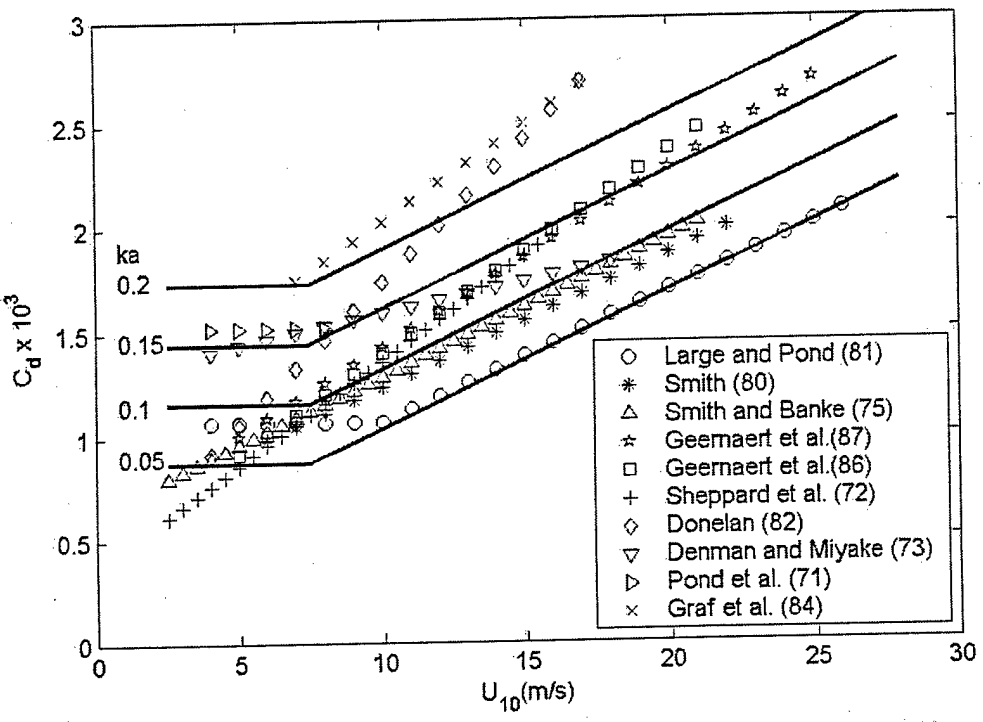

Fig. 2 Comparison of Equation (1) with the drag coefficient formulas complied by Geernaert (1990).

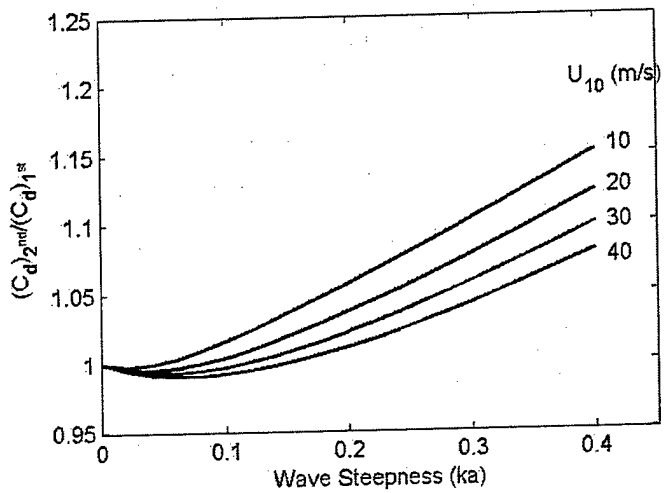

Fig. 3 Effects of wave steepness and wind speed on the drag coefficient

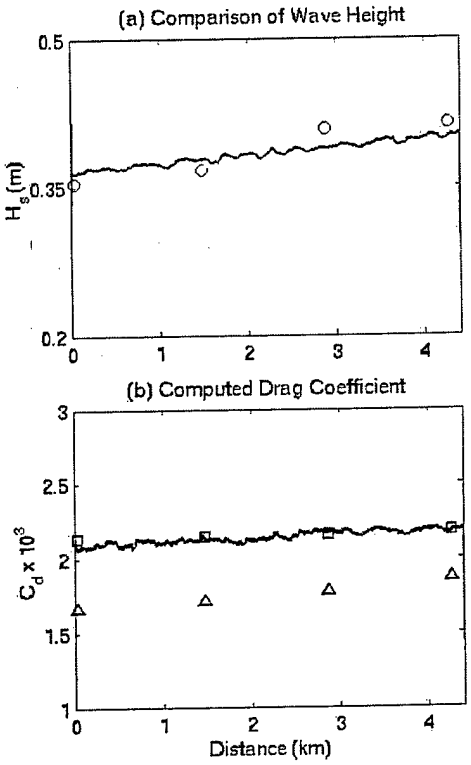

Fig. 4 Comparisons of the computed and measured significant wave heights (top), and the computed and inferred drag coefficients (bottom) in the case of U_{10} = 10.8m/s. Solid lines: Boussinesq model results, circles: Young and Verhagen's (1996) observations, squares: Anctil and Donelan (1996), and triangles: Taylor and Yelland (2001).

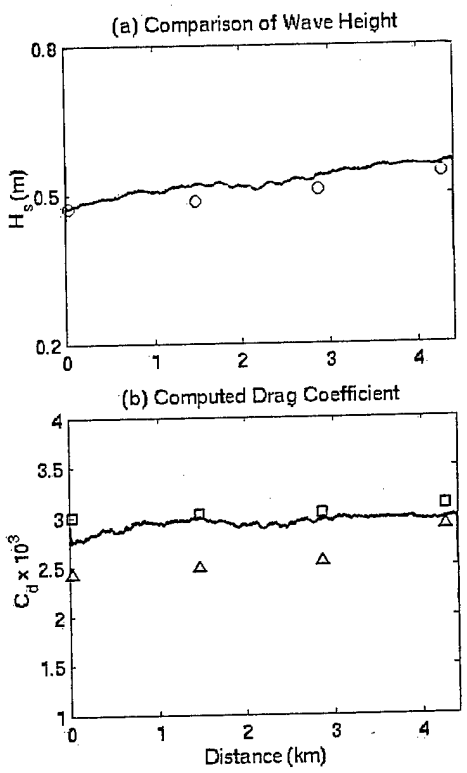

Fig. 5 Comparisons of the computed and measured significant wave heights (a) as well as the computed and inferred drag coefficients (b) in the case of U_{10} = 15.2m/s. Solid lines: Boussinesq model results, circles: Young and Verhagen's (1996) observations, squares: Anctil and Donelan (1996), and triangles: Taylor and Yelland (2001).

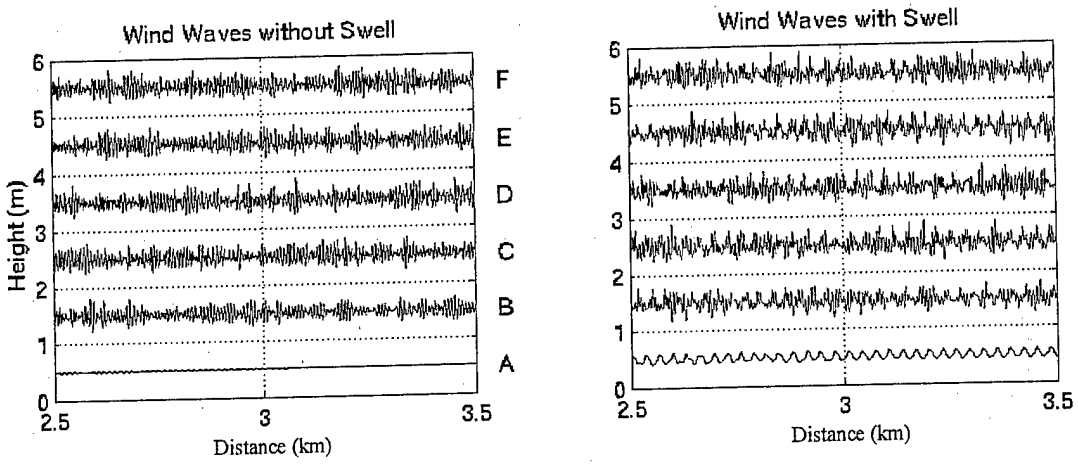

Fig. 6 Snapshots of modeled sea surface without (left) and with (right) swell

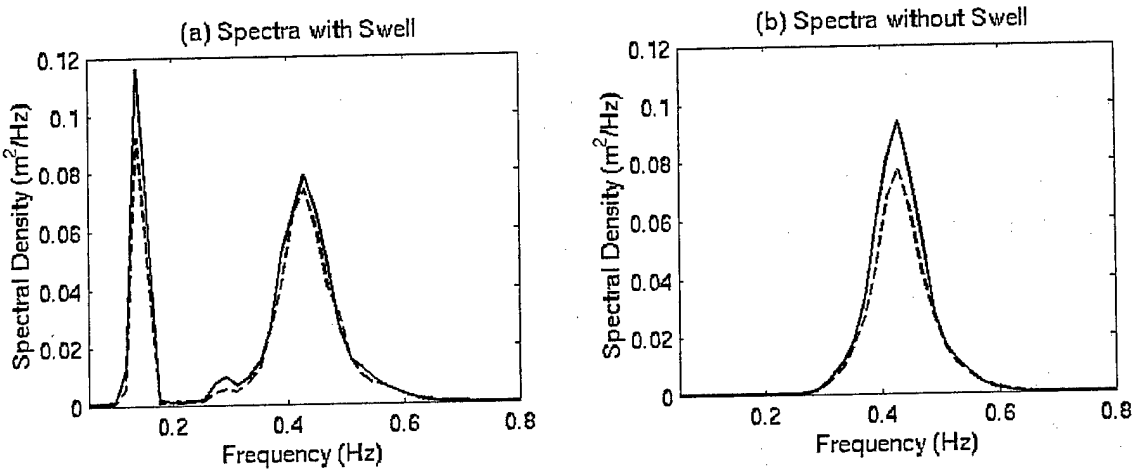

Fig. 7 Suppression of wave growth by the ambient swell (left). Dashed lines: up-wave boundary, solid lines: 4 km down-wave.

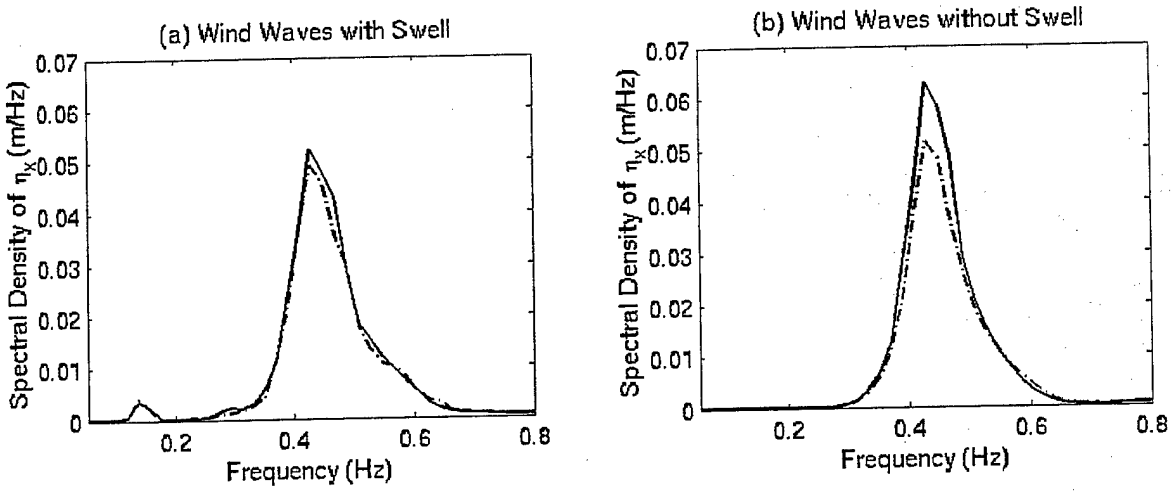

Fig. 8 Spectra of sea surface slope with (left) and without (right) swell. Dashed lines: up-wave boundary, solid lines: 4 km down-wave.

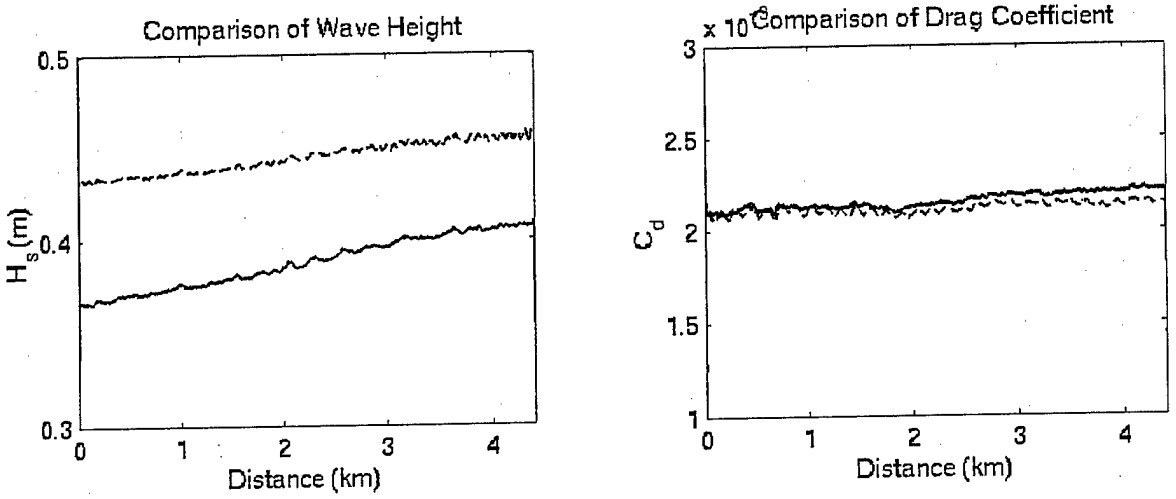

Fig. 9 Effects of swell on wave height and drag coefficient. Dashed lines: sea and swell, solid lines: short waves.

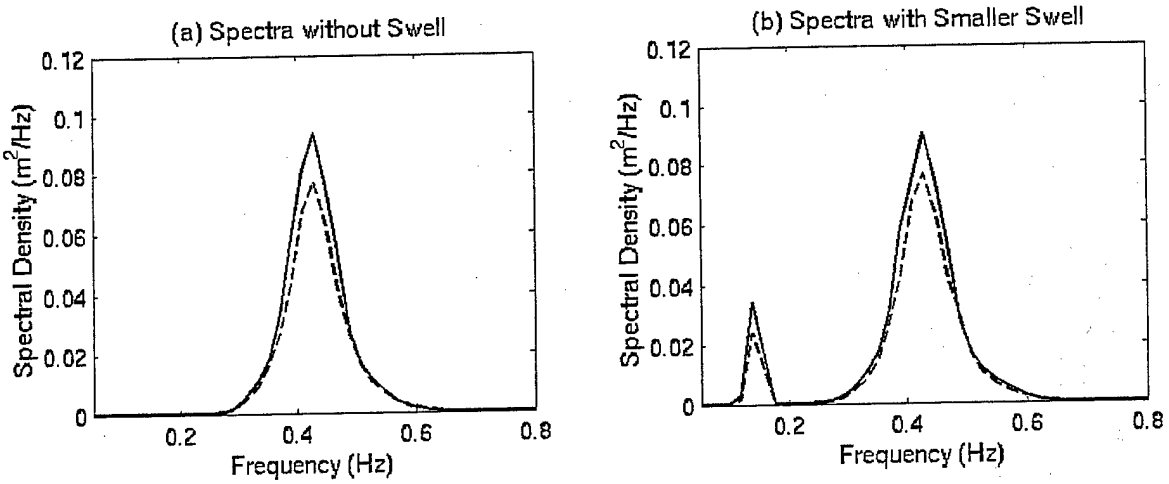

Fig. 10 Suppression of wave growth by the swell (left) with a small amplitude. Dashed lines: up-wave boundary, solid lines: 4 km down-wave.